land

Article

Simulation of Urban Areas Exposed to Hazardous Flash Flooding Scenarios in Hail City

Omar Hamdy [1,*], Mohamed Hssan Hassan Abdelhafez [2,1,*], Mabrouk Touahmia [3], Mohammed Alshenaifi [2], Emad Noaime [2], Khaled Elkhayat [2], Mohammed Alghaseb [2] and Ayman Ragab [1]

1 Department of Architectural Engineering, Faculty of Engineering, Aswan University, Aswan 81542, Egypt
2 Department of Architectural Engineering, College of Engineering, University of Hail, Hail 2240, Saudi Arabia
3 Department of Civil Engineering, College of Engineering, University of Hail, Hail 2240, Saudi Arabia
* Correspondence: omar.hamdy@aswu.edu.eg (O.H.); mo.abdelhafez@uoh.edu.sa (M.H.H.A.)

Abstract: According to the United Nations (UN), an additional 1.35 billion people will live in cities by 2030. Well-planned measures are essential for reducing the risk of flash floods. Flash floods typically inflict more damage in densely populated areas. The province of Hail encompasses 120,000 square kilometers, or approximately 6% of the total land area of the Kingdom of Saudi Arabia. Due to its innate physiographic and geologic character, Hail city is susceptible to a wide variety of geo-environmental risks such as sand drifts, flash floods, and rock falls. The aim of this work is to evaluate the rate of urban sprawl in the Hail region using remote sensing data and to identify urban areas that would be affected by simulated worst-case flash floods. From 1984 to 2022, the global urbanization rate increased from 467 to 713% in the Hail region. This is a very high rate of expansion, which means that the number of urban areas exposed to the highest level of flood risk is rising every year. With Gridded Surface Subsurface Hydrologic Analysis (GSSHA), a wide range of hydrologic scenarios can be simulated. The data sources for the soil type, infiltration, and initial moisture were utilized to create the coverage and index maps. To generate virtual floods, we ran the GSSHA model within the Watershed Modeling System (WMS) program to create the hazard map for flash flooding. This model provides a suitable method based on open access data and remote data that can help planners in developing countries to create the risk analysis for flash flooding.

Keywords: urban area; flash flood; remote sensing; GIS; GSSHA; Landsat; historical event; natural disasters; urban exposure

Citation: Hamdy, O.; Abdelhafez, M.H.H.; Touahmia, M.; Alshenaifi, M.; Noaime, E.; Elkhayat, K.; Alghaseb, M.; Ragab, A. Simulation of Urban Areas Exposed to Hazardous Flash Flooding Scenarios in Hail City. *Land* **2023**, *12*, 353. https://doi.org/10.3390/land12020353

Academic Editors: Domenico Calcaterra and Troy Sternberg

Received: 15 November 2022
Revised: 12 January 2023
Accepted: 20 January 2023
Published: 28 January 2023

1. Introduction

The rapid population expansion and rural flights to urban areas and cities have led to dramatic shifts in urban landscapes in recent decades [1]. By 2030, the United Nations predicts 1.35 billion more people will be living in urban areas, bringing the total to almost 5 billion. Moreover, the area of developed land throughout the world is expected to grow by 1.2 million square kilometers, or almost three times as much as it was in 2000 [2]. Changes in land use and land cover are common results of urbanization everywhere, but notably in poor nations [3]. Further, cities tend to expand in all directions, sometimes even into more hazardous locations. Consequently, this issue should be lessened by decision-makers and planners through risk management and the provision of various options.

Urban sprawl is a sort of low-density development that includes residential, retail, and office districts; it is also a measure of the rate and direction of urban expansion. In fact, it is fair to classify any expansion toward the suburbs as urban sprawl [4,5]. Sprawl in cities is a key topic in urban studies right now [6]. As urbanization spreads to formerly undeveloped areas, planners and policymakers in emerging nations are beginning to pay more attention to the phenomenon and its effects [5]. Global urbanisation is accelerating. Population growth necessitates urban development. However, throughout the last century, metropolitan areas grew faster than populations globally, especially in developing countries where growth is often unplanned and uneven [7–9]. Between 2000 and 2005, an average of 240 million people were affected by natural disasters annually globally. This is a startling increase in both the frequency and intensity of catastrophes. Natural catastrophes increased to 414 in 2007, resulting in the deaths of 16,847 people, injuries to over 211 million people, and displacement of over 110 million more [7]. Increases in the rate of climate change have been linked to an increase in the frequency of extreme weather occurrences. The rising frequency of natural disasters worldwide was again documented in 2014. The rise in reported hydro-meteorological disasters is a major factor in this pattern. This trend is mostly attributable to hydrological (mainly floods) and meteorological (mainly storms) disasters. The frequency of recorded hydrological catastrophes has been rising at a rate of 7.4% per year during the past few decades. A rising population is a growing threat, and from 2000 to 2007, the yearly growth rate of the world's human population was 8.4%, [7], therefore the number of people in danger rose. Floods and droughts are increasing due to climate change. Climate change has increased the likelihood and severity of extreme weather events such as floods and droughts. Compared to 1.5 °C global warming without adaptation, direct flood damage increases by 1.4 to 2 times at 2 °C and 2.5 to 3.9 times at 3 °C [8]. Hoegh-Guldberg et al. (2018) predicted with medium confidence that 2 °C global warming would increase flood threats relative to 1.5 °C. Urban growth will increase flood-prone areas by 2.7 times by 2030, according to Guneralp et al. (2015) [9].

In a sense, a flash flood is a local flood that occurs suddenly and lasts for only a short time after strong or extreme rainfall (often less than six hours) [8,10]. After intense rainfall, rivers, streets, and even gorges in the mountains can become inundated by roaring torrents that wash away everything in their path [11]. When it comes to predicting the timing and location of natural disasters, the flash flood phenomena are among the most challenging. Due to this, it can be difficult for relevant authorities and communities to respond adequately; well-thought-out preparations for doing so are essential for reducing the risk of flash [10,12]. Risk assessment is the backbone of any study into the probable costs of a catastrophe. For a specific location and period of reference, the risk is defined as the potential for loss (of lives, injuries, property damage, and interruption of economic operations) [13]. Risk is made up of three components: hazard, exposure, and vulnerability. Data from each of these areas can be utilized to construct a picture of risk in a specific location and over time. These elements are as follows: (1) Hazard—a potentially harmful physical phenomenon (e.g., an earthquake, a windstorm, a flood). Natural risks such as flash floods and landslides are common. (2) Exposure—the location, characteristics, and value of assets that are vital to communities (people, buildings, industry, farming, all land uses, etc.) and that could be affected by a hazard. (3) Vulnerability—the risk that assets will be damaged/destroyed/affected when exposed to a hazard. For example, an elderly person may be more exposed to the effects of floods because he or she has a more difficult time fleeing or relocating rapidly [11,14]. Losses from flash floods tend to be greater in highly populated regions. When there is a lot of rain, the storm drains may fill up and flood the streets and nearby buildings [10,15]. Also, sites where rainwater collects, such as urban streets and rooftops, pose a greater threat [15]. The water level in rivers and streams can suddenly increase, and the flow velocity can be quite fast, causing significant damage to anything in its path, including rocks, trees, bridges, and structures. As a result, life and property are in grave danger from flash floods [10]. Assessing risk is the backbone of any assessment of catastrophe preparedness costs. The death toll from flash floods tends to be higher in more populated areas. Storm drains have been known to overflow during times of severe rainfall, causing flooding of streets and houses [15]. Most passenger cars can be swept away by a strong river even at a depth of 60 cm [10]. In addition, metropolitan areas are at significant risk because of the accumulation of rainwater runoff on the ground, streets, and rooftops. The water level in rivers and streams can suddenly rise, and the flow velocity can be quite fast, causing significant damage to anything in its path, including rocks, trees, and even structures. As a result, life and property are in grave danger from flash floods [10].

Following on from the CASC2D model [16], the Gridded Surface Subsurface Hydrologic Analysis (GSSHA) model is a gridded, distributed, and physically based hydrologic model. Overland flow and channel flow in one dimension are simulated using explicit finite-volume solutions of the diffusive wave formulation of the St. Venant equations of motion in two dimensions on a structured grid [17]. Ogden, Downer, and Meselhe illustrate the GSSHA program's ability to accurately model a wide range of hydrologic conditions. Individual models can also be altered much more easily using GSSHA than with other approaches [18]. Aside from GSSHA, numerous other existing numerical models for simulating flood events exist, such as MIKE FLOOD, FLO-2D, CCHE, and TUFLOW. None of the above flood models have been connected with a GIS in such a way that a user may quickly adjust boundary conditions, execute, and archive a flood simulation for various levee breach scenarios into a geodatabase. Indeed, one goal of this research was to create such a system [19]. For a given set of hydrometeorological inputs, the model can simulate the watershed's resulting hydrologic response [20]. GSSHA is utilized because it is the only model that considers the geographical variability of land-surface and hydrodynamic characteristics, including underground storm drainage systems. Increases in drainage density, especially from low levels, have been found to result in much higher flood peaks [21].

In terms of hydrology, GSSHA is a geographically dispersed, physics-based, continuous simulation model. With GSSHA, calculations are performed on a standard raster grid that stands in for the watershed network in question. Within each grid cell of the model, at a user-defined time step, the model numerically simulates a wide variety of hydrologic processes, including the distribution of rainfall, evapotranspiration (ET), infiltration, surface water retention, overland flow runoff, and snowmelt/accumulation. Although these hydrologic processes are simulated locally within each cell, their interconnectedness via 2D overland flow, 2D groundwater flow, and a 1D stream network allows for simulations of the watershed response as a whole [22,23]. The two primary elements of this project were the GSSHA model and the Watershed Modeling System (WMS), a graphical user interface (GUI) that offers pre and post-processing for the GSSHA model. The Engineer Research and Development Center (ERDC) of the U.S. Army Corps of Engineers and Aquaveo, LLC are actively developing and refining both programs [23]. The GIS-based user interface of WMS allows for both pre- and post-processing of digital spatial data, which is essential for hydrologic modelling and visualization [22]. The verification of the simulation in this paper is primarily based on the verification of the WMS software and the GSSHA model. This is because this research does not change any equations of the GSSHA model; rather, it merely provides the model with the necessary data for the study area.

In the last ten years, remote sensing technology has evolved substantially, allowing for more nuanced descriptions of urban surveillance. Due to its usefulness in inventory evaluation and monitoring of environmental assets based on spatial data, remote sensing data is increasingly being used in a variety of sectors [24,25]. The governments of developing countries generally struggle to keep their databases up to date using traditional techniques due to the time and cost involved [4]. This makes remote sensing applications especially important. Moreover, urban land use may be identified with the use of remote sensing data [26]. There is a plethora of satellite imaging data, including but not limited to Landsat, IKONOS-2, and OrbView-3 (commercial data). Spectral satellite data is available for relatively long time periods and sufficient precision, although Landsat has been chosen as the best option for monitoring spatial details [27]. Free and easily downloadable from the US Geological Survey's website, Landsat data [28] may give primary results that are close to real-world conditions [29] and capture landcover change in urban and peri-urban environments [30].

The Kappa coefficient [31,32] is one of the most often used strategies for determining the level of agreement across datasets to validate the correctness of supervised classification [33–35]. This may be used to ensure that the categorized Landsat imagery is correct.

To evaluate a categorized map's precision, we generate random points using ground truth points and then compare them to actual classifications in a confusion matrix. As imagery at these resolutions allows viewers to easily differentiate between main natural land cover classes and to detect components of the developed environment, such as individual residences, industrial buildings, and highways, Google Earth is frequently used to evaluate ground truth points [36–38]. Both the user and the supplier may be evaluated for accuracy in each class, as well as for overall agreement using the Kappa index [39], these scores range from 0 to 1, with 1 representing perfection [40].

Due to its innate physiographic and geologic character, the Hail desert in Saudi Arabia is susceptible to a wide variety of geo-environmental risks. These risks include sand drifts, flash floods, rock falls, problematic soils, and the possible dangers posed by intra-plate lava flows from dormant volcanoes (also known as harrat) are all included in this list of potential dangers. Both remote sensing and on-site investigations were carried out to locate and assess the severity of these dangers. The region of Hail is experiencing rapid urban and agricultural expansion, yet some infrastructure has been built in sites that are susceptible to being damaged by geo-environmental hazards. When it comes to the implementation of sprawl and the increase in public services, development plans should take such dangers into consideration [41]. Using remote sensing methods, several earlier investigations were conducted in Saudi Arabia to investigate the geologic dangers that are present in the nation [42]. IKONOS data were applied to map the danger of flash flooding in the Jeddah region along the coast of the Red Sea [43]. To map the sabkha soils in the Jazan region, Landsat and QuickBird photos were employed [44]. Using satellite data, there is an ability to bring attention to sand dune accumulations in the general vicinity of the city of Riyadh [45]. SPOT satellite data and digital elevation models were used to estimate the risk of landslides occurring over the border between Saudi Arabia and Yemen [41].

The challenge of examining the exposure of urban areas to the dangers of flash floods represents an important point that inspired this research to test a method of researching this problem by re-simulating the worst flash floods that landed in the study area. Thus, the purpose of this paper is to address two key issues for urban growth management. These issues are (i) estimation of the pace of urban sprawl of Hail city periphery using remote sensing data and (ii) identification of urban areas located in regions that will be affected by simulated the worst case of flash floods that happened in the historical events in the case study area between the years of 1982 and 2022. Both issues are important for urban growth management in developing countries where there is a lack of data.

2. Study Area

Hail city, the region's capital, is in northern Saudi Arabia, near the intersection of the Arabian Shield and the Arabian Platform [46]. The Hail region lies between 40° E to 42°30 E and 26°50 N to 28°33 N [47] and encompasses 120,000 km^2 which accounts for 6% of the Kingdom of Saudi Arabia. It is situated in the KSA's center north as shown in Figure 1 [48,49].

The region is characterized by a hot dry desert, with a yearly rainfall of less than 250 mm and annual evaporation rates of up to 3000 mm/year [50]. Whereas average yearly temperatures range from 10 °C in winter to 32 °C in summer [41]. Summer is hot, with high temperatures and low relative humidity in August [46]. Torrential rain that fell on the city of Hail caused a massive loss of money, property, and lives and claimed the lives of many families that have not been tallied in the absence of a torrent discharge and projects to ward off risks. Moreover, adult house valleys that permeate the city of Hail route were not considered during the implementation of residential plans over the previous thirty years [51].

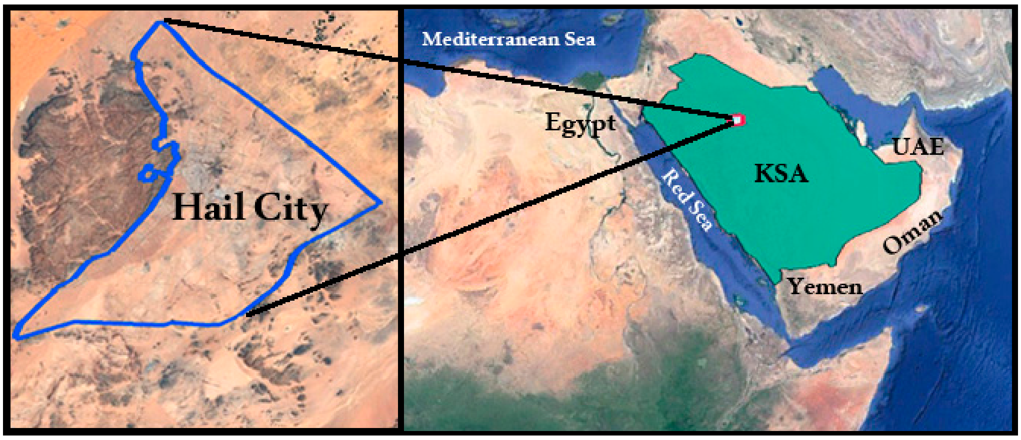

Figure 1. The location of the study area (Hail City).

Due to its inherent physiographic and geologic character, the Hail desert is exposed to a variety of geo-environmental dangers. Sand drift, flash floods, rock falls, issue soils, possible risks from dormant volcano intra-plate lava flows (harrat), and dust storms are among the threats. These dangers were identified and quantified using remote sensing and field inquiry. Hail is a developing urban and agricultural region, yet some infrastructure has been built in geo-environmental hazard-prone areas. When implementing sprawl and the increase in public services, development plans should account for such risks [41]. Hail city is built on a complicated network of wads, which causes floods on a regular basis. Due to present growth tendencies, several urban systems, including 29% of city roadways and 24% of built-up regions, as well as farmlands within the 1450 UGB, are in danger of flooding. As a result, flood protection limits must be appropriately defined across the city to prevent growth in flood-prone regions, as well as proper standards for preserving water supplies [52]. Flash floods are a substantial contributor to Saudi Arabia's water resources. However, the land is mainly dry [53].

Hail has a population of 345,000 inhabitants and an average population density of 19.63 p/ha within the current built-up area. The total built-up area of the city covers 7634 ha. Only 4% of the built-up area supports a density above 50 p/ha and accommodates 13% of the population, whereas 3.7% of the total built-up area has a population density between 30 and 50 p/ha and accommodates a further 9% of the population [52].

3. Research Methodology and Simulation Data

The purpose of this article is to map out the areas of the case study area most likely to be impacted by floods and to inquire into the connection between those areas of high risk and urban sprawl. The collected data would be sent into the WMS program where it would be utilized to mimic the torrent and runoff water allowing high-risk regions to be pinpointed.

3.1. Simulation Data Sources

The research goals could not be met without the inclusion of specific information. The accessible statistics for the case study area were lacking, however. For instance, we were unable to undertake a thorough examination of urban sprawl since the government's comprehensive plan did not include data on when the structures in the urban regions were completed. The second issue was the poor quality of free, publicly available materials such as Land Use maps, soil types maps, and DEM (digital elevation models). It was rather pricey to obtain high-resolution DEM data. The third issue was how hard it was to obtain official government statistics on the case study location. Most simulation settings and parameters provided and connected to the study region were chosen and recommended from the manual of model software. The origins of all simulation data files are listed in Table 1.

Table 1. Data used in flood simulation.

	Data Source
Urban Area	Landsat satellite images.
DEM file	U.S. Geological Survey (USGS) Website.
Land Use map	USGS Land Cover Institute.
Soil Type map	Food and Agriculture Organization of the United Nations (FAO) Digital Soil Map of the World (DSMW).
Precipitation	Literature Review.

As can be seen in Figure 2, digital elevation models (DEM) are a valuable data source for GIS. They have found widespread use in surface hydrology modelling, namely in the form of automated catchment area delineation [54]. This research made use of the two most popular satellite-derived DEM datasets (SRTM and GDEM). With a horizontal grid size of just 3 arc-seconds (or 90 m), SRTM can give almost worldwide topographic coverage of the Earth. One-second (30-meter) statistics for all of Earth, excluding the Middle East, were made public just recently [55]. The quality and resolution of digital elevation models (DEMs) are crucial for hazard assessments and inundation modelling of coastal areas [56]. The approach used in this article was affected by the outcomes of the aforementioned three issues because of data gathering restrictions. By analyzing Google Earth's archived photos, we were able to solve the first issue of insufficient data on the building's construction year. We exploited the low-resolution but free web data to overcome the second issue of high-resolution imaging acquisition expenses. The WMS program helped us get our hands on a free Land Use map, Soil Type map, and DEM data. Thirdly, we used information gathered from published studies and reports from our own institutes to address the challenge of acquiring topographic coverage of the research region.

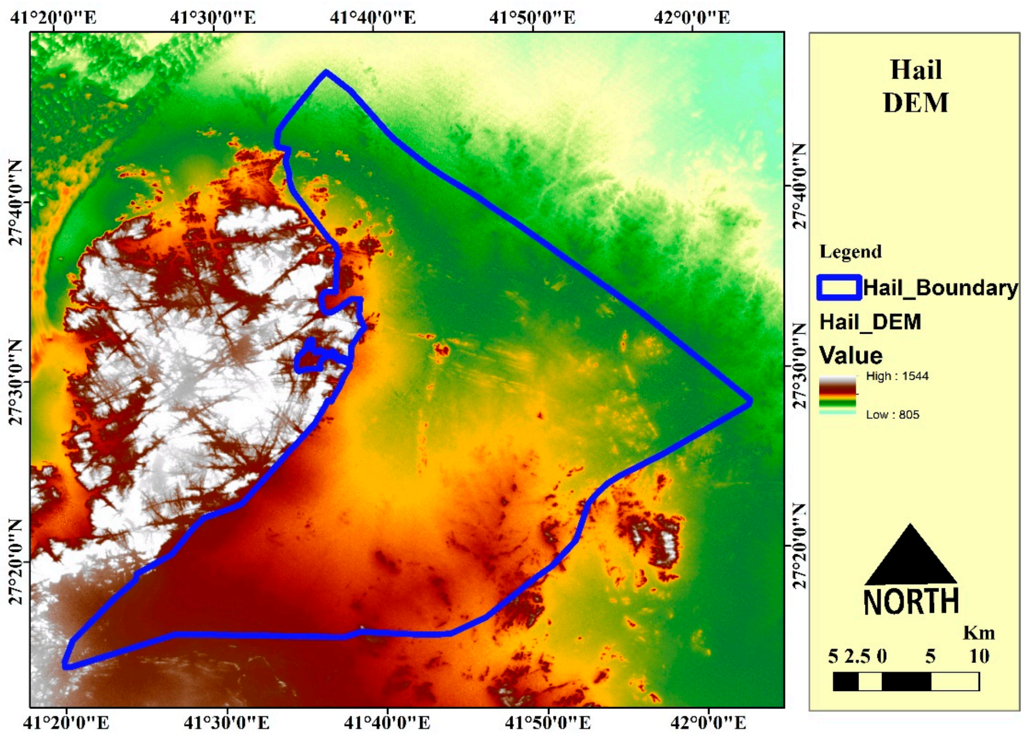

Figure 2. Digital Elevation Model file for the case study area.

3.2. Identifying Urban Areas

To classify an image, it must be converted from a multiband raster image to a single-band raster with a variety of classification groups that correspond to different types of land cover [57]. Two primary methods exist for classifying a raster image with several bands: supervised and unsupervised. It is a pretty typical strategy for researchers to evaluate remote sensing data to categorize images into their respective land cover classes. The supervised classification method makes use of spectral signatures from training polygons that stand in for distinct sample regions of the various land cover classes. To classify the image, the image analyzer takes samples from it. When using an unsupervised classification method, the software finds the spectral classes in the multi-band image without any assistance from a human analyst. Once clusters have been found, the next stage is to determine what they represent (water, desert, etc.) [57].

The years of study for this research were chosen to extract land uses by determining the worst flash flood phenomenon that has ever occurred in the past in the city of Hail, which was in 1981. However, this year no images were available from Google Earth until the Kappa validation was performed, so the year that is closest in which Landsat images are available was chosen instead. In addition to that, there are images of it on Google Earth from 1984, the year in which the research was conducted on it. Regarding the most recent land usage, the year 2022 has been selected as the one in which to investigate the effect that flash floods have on urban areas.

3.3. Identifying the Risk Areas

This section's approach explains the selection criteria used to pinpoint potential danger spots. At first, the cities were divided into two zones. One half was designated as the safe zone, which would not be affected by floods caused by torrents or runoff after a severe downpour, while the other half was designated as the danger zone, into which massive volumes of rainwater would flow after a storm. We simulated precipitation and runoff from the area's surfaces using the GSSHA model in WMS software to arrive at this categorization. Figure 3 depicts the entire simulation process. The runoff depth was shown on a depth map that was the primary product of the simulation. If the map were exported to the Arc GIS format, a polygon layer would be created for each depth range. The potential hazards were then subdivided into five categories according to water depth. Very low danger was defined as a flood depth of less than 0.5 m, low hazard as 0.5 m to 1.0 m, medium hazard as 1.0 m to 2.0 m, high hazard as 2.0 m to 5.0 m, and extreme hazard as >5.0 m [38].

Ogden et al. illustrate the versatility of the GSSHA software in simulating a broad variety of hydrologic conditions. Moreover, unlike other methods, GSSHA makes it simple to modify certain models [18]. In addition to GSSHA, there are a plethora of other pre-existing numerical models that may be used to simulate flooding. Rapid estimates of the damage caused by floods due to a breached levee can be made with a one-dimensional model. In contrast to two-dimensional models such as MIKE FLOOD, CCHE, FLO-2D, and TUFLOW, its predictions tend to be off. A two-dimensional model's main drawback is the time it takes to create. If computers could process information faster, this disadvantage would be far less severe. For Windows, GSSHA is written in C++ and soon Linux will have support for parallel processing. A user can utilize many computers or processing cores in parallel to execute a single flood simulation. Making use of this method in GSSHA can drastically cut the time it takes for the model to run. All the aforementioned flood models lack GIS integration that would allow a user to easily change boundary conditions, run a flood simulation, and save the results in a geodatabase in case of a levee break. Indeed, the creation of such a system was one motivation for our study [58].

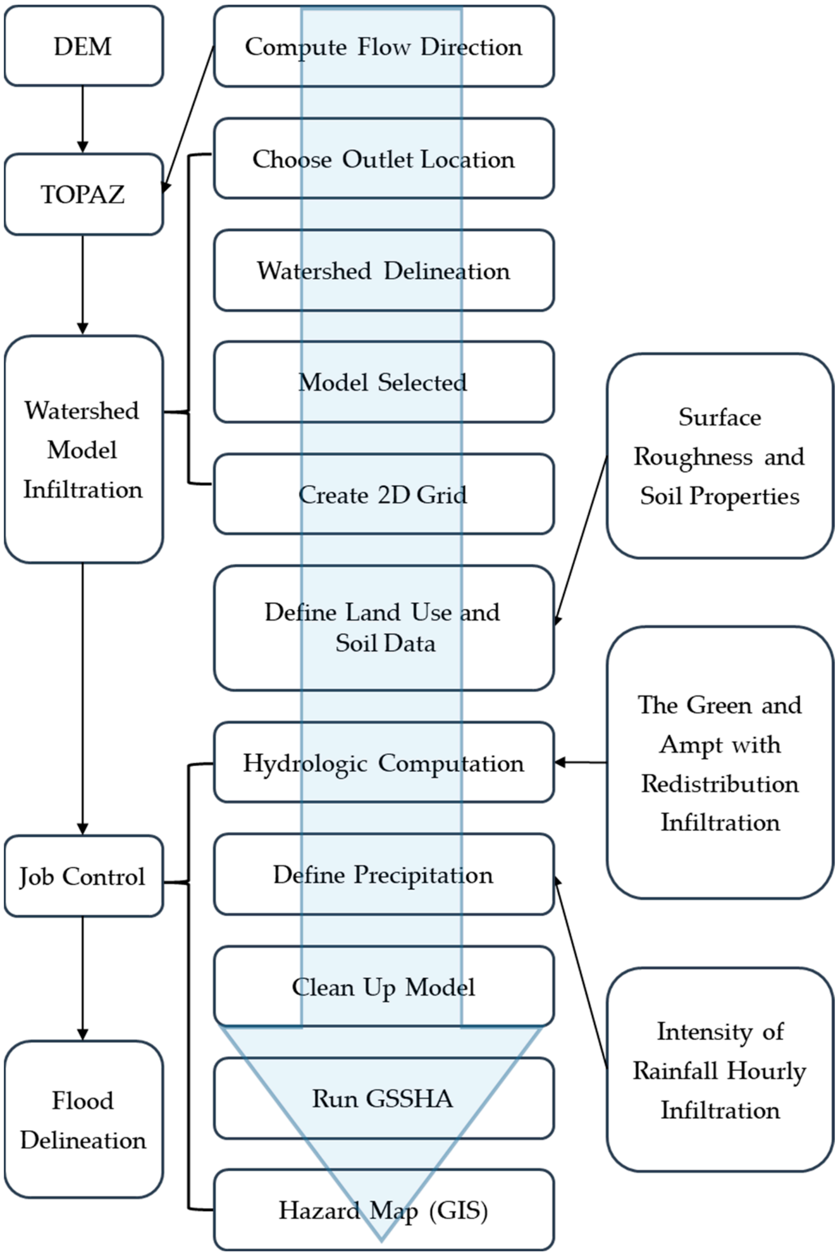

Figure 3. Simulation steps.

For hydrologic and hydraulic modelling, WMS can handle any kind of GIS data. WMS gives the user a robust set of tools for working with vector and raster data in a geographic information system. The WMS can automatically calculate a wide variety of hydrologic characteristics. These include area, slope, mean elevation, maximum flow distance, and many more. In addition, developing a GSSHA model with WMS is the quickest and easiest option. Setting up the files for a GSSHA model has never been easier with this helpful tool. The Hydrologic Modeling Wizard in WMS makes it simple to develop a basic GSSHA model from scratch by walking you through the necessary steps. The creators of the GSSHA have advocated for the usage of WMS in both the preliminary and final stages of the processing pipeline. It also makes project visualization easier, which speeds up the process of setting up a GSSHA model. Due to these considerations, WMS was employed in this investigation for both model development and analysis [18,58].

3.4. Classifying Urban Areas Exposure

In this critical segment of our research methodology, we had to determine which parts of the case study area would experience flash floods in relation to its location from the hazard area classes. To achieve this objective, we used Arc GIS software to analyze the data from the WMS simulation. A supervised classification map for the case study area was detected, with an overlay of the urban area which was divided into five sections; land use was in an area subjected to simulated floods of varying degrees, and runoff water at different depths. In this deluge, the flood depth that was simulated in the areas that were going to be flooded was used to generate the hazard for the area that was being studied. The risk assessment was performed using the guidelines provided by the Ministry of Land, Infrastructure, and Transport of Japan (MLIT), which are detailed in Table 2 [38].

Table 2. Flood hazard classification according to MLIT [38].

Flood Hazard	Hazard Degree	Depth (Meters)
H1	Very Low	<0.5
H2	Low	0.5–1
H3	Medium	1–2
H4	High	2–5
H5	Extreme	>5

4. Simulation Process

Delineating and characterizing watersheds, which is the first step in GSSHA modelling, is necessary because it establishes the scope of the issue at hand. The fundamental order of operations for using GSSHA for distributed hydrologic modelling is as follows. The TOPAZ system was initially implemented. Acquiring digital elevation data for the watershed of the research region allowed us to calculate flow direction and accumulation. Infiltration in watershed models was also analyzed. This phase involved four procedures: (i) choosing an outlet point, (ii) defining the watershed, (iii) starting the model, and (iv) generating a 2D grid. In the third phase, GSSHA job control guidelines were established. Index map generation from land use and soil data, starting parameter values for index maps, and precipitation definition all had three inputs. The model was then cleaned up and run via model 4 after going through all these steps. Finally, utilizing the WMS data based on water depth, a danger hazard map was generated in Arc GIS [19].

4.1. Extraction of DEM for the Study Area's Watershed

The user can define a search region and choose a desired data resolution before obtaining the results from the USGS through online services. Classifying runoff and infiltration characteristics required the DEM in addition to land use and soil type data. The soil types were obtained from the Soil Data Mart, which may be found at soildatamart.nrcs.usda.gov (accessed on 14 November 2022) [59].

4.2. Land Use and Soil Data

The FAO soil classification system was used to identify soil types, and the USGS Land Cover Institute database was consulted for land use information (Landsat supervised classification). We constructed coverage and index maps from these two data sets. The index map table was made to accommodate the various land cover and soil hydrological factors present in the watershed. Consequently, various parameters were allocated to each grid cell based on the land cover and soil type [60]. Soil maps are displayed in Figure 4.

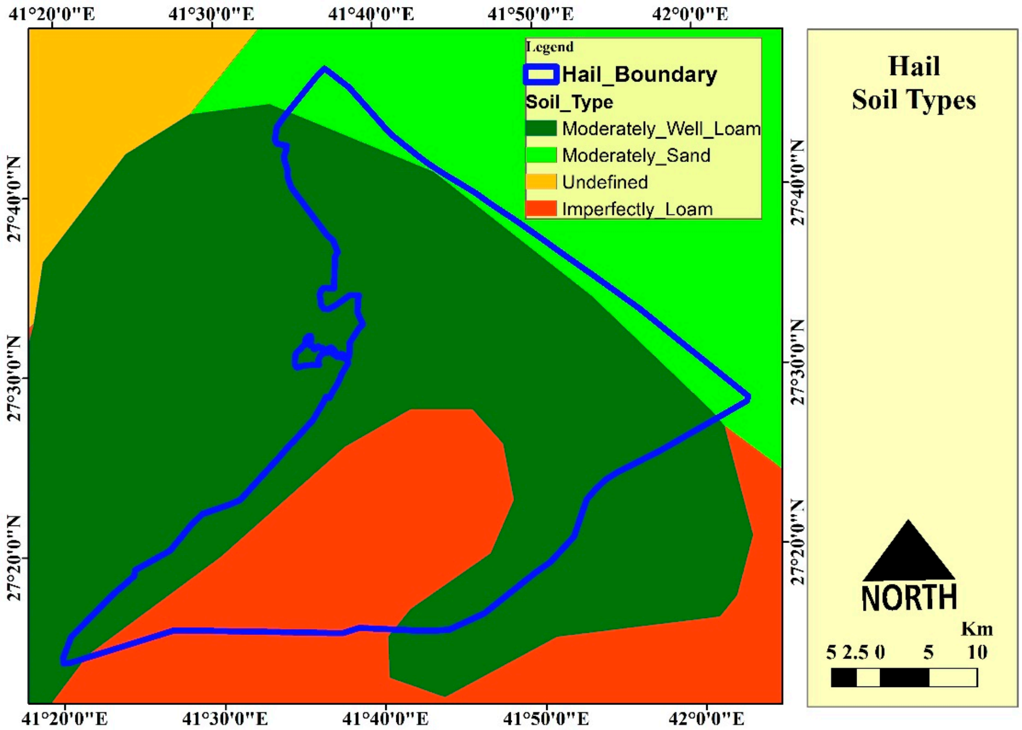

Figure 4. Soil type map for Hail city.

4.3. Infiltration and Initial Moisture Data Source

Land cover value estimates based on basin roughness may be found in detail on the GSSHA wiki. The GSSHA wiki was used to determine the manning roughness coefficient for each land cover type in the watershed basin. When water permeates the soil from the ground up, it is called infiltration. The GSSHA work order management system mandates the use of an infiltration strategy. Therefore, the Green and Ampt soil moisture redistribution technique was adopted for this project. Individual identifiers for the soil type index map were constructed while infiltration was taken into consideration [18].

The percentage of water volume already present in the soil is referred to as its initial moisture. Preliminary moisture levels range from one set of criteria to another. Since soil type and time of year were the two most influential elements, the results were not constant. The starting moisture value should be chosen such that it is not more than the soil's porosity.

4.4. Rainfall Values

Assigning constant values for precipitation over the whole watershed was kept primarily as a diagnostic tool and was utilized extensively during the early stages of model development. The input parameters for uniform rainfall throughout space and time were as follows: (1) rainfall intensity (mm/h) and (2) rainfall duration (minutes). This work simulated the first parameter in the most extreme conditions in historical events (1981), with rainfall rates of 79.6 mm/h. [51,61]. For the second parameter, which determines how tiny an area is in danger, we settled on a value of three hours (180 min) as an average duration of all watersheds in the study area, even though the range of possible rainfall durations in Hail is three hours [61].

5. Results

This section will describe the study's findings in three sections, each displaying different findings based on the type of analysis used. The first section will present the results of the method used to identify historical urban areas in specific years. The second section will depict the flash flooding results in greater detail, classifying the risk zones based on water depth. The last section will look at how the results of the other sections overlap in order to find out which urban areas are at risk of flash flooding and compare how exposed urban areas were in 1984 and 2022.

5.1. Urban Land Use

This section will present the results of a Landsat analysis to extract the land uses in 1984 and 2022. Landsat satellite images provide a helpful approach to strewing historical urban areas. Figures 5 and 6 show the results of the first stage, which started in 1984 and 2022 with the integration of bands for the case study area. The colors used in this illustration are those seen in nature, and there is no atmosphere present. The identical image is shown in Figures 7 and 8, but after it has been submitted to supervise categorization through the use of GIS.

In order to evaluate the results of applying supervised classification to the Landsat satellite images, a classification accuracy assessment is an essential step that must be taken. The accuracy test for the 1984 and 2022 land use maps used a total of 500 random test sites for each one that was dispersed across the categorized groups to evaluate the classification accuracy. This can be seen in Figures 9 and 10, which show how the accuracy test was carried out. The Kappa coefficients were determined by doing calculations based on the error matrices that were developed. The accuracy of class categorization ranged from 0.94 for urban in 1984 to 0.93 for urban class in 2022, as shown in Table 3 for 1984 and Table 4 for 2022. The accuracy of class categorization for non-urban areas was 0.98 for 1984 and 0.99 for 2022, resulting in a total accuracy of 88 percent for 1984 and a Kappa value of 92 percent for 2022, which demonstrates that classification accuracy is extremely reliable [62].

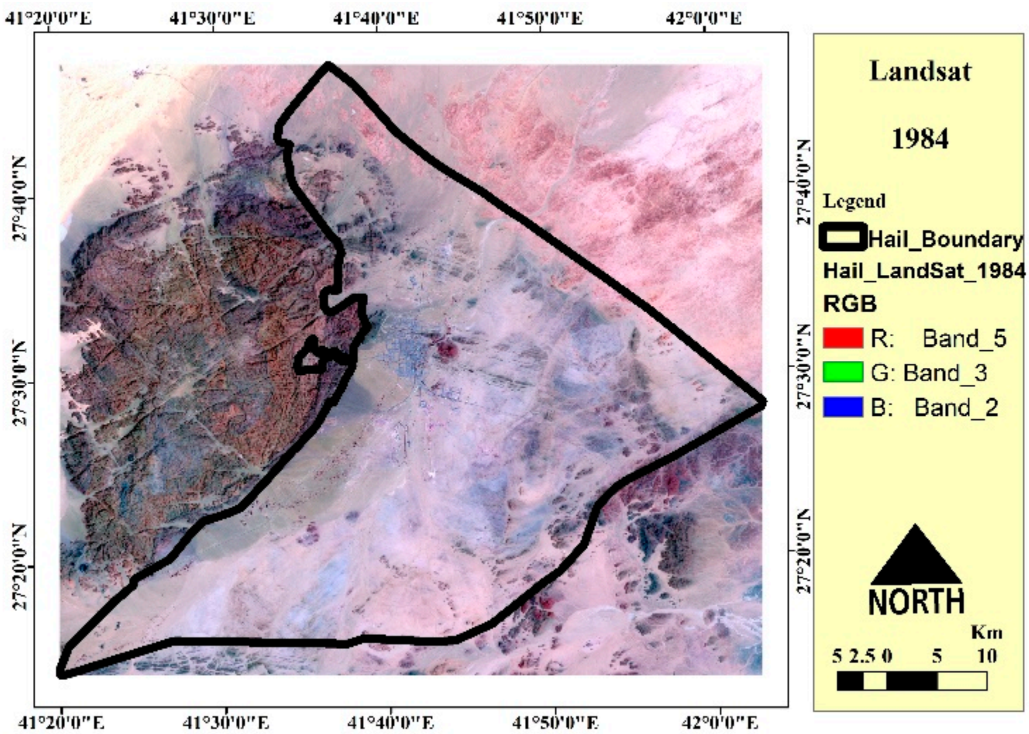

Figure 5. Satellite image (Landsat 1984) for the study area.

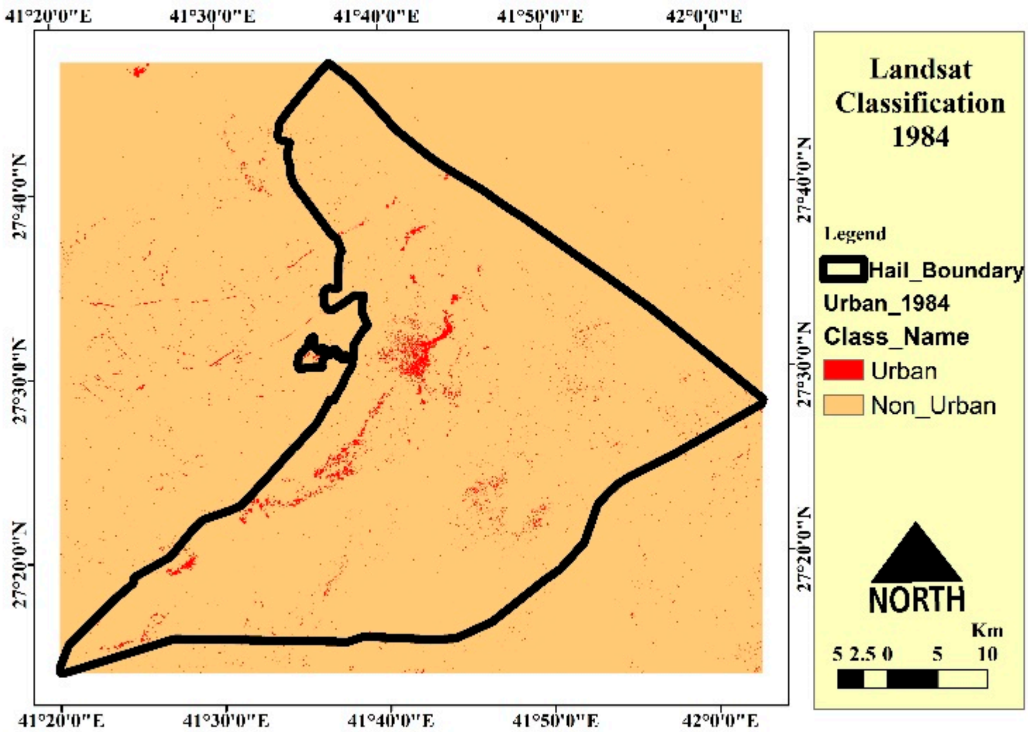

Figure 6. Landsat classification for an urban area, 1984.

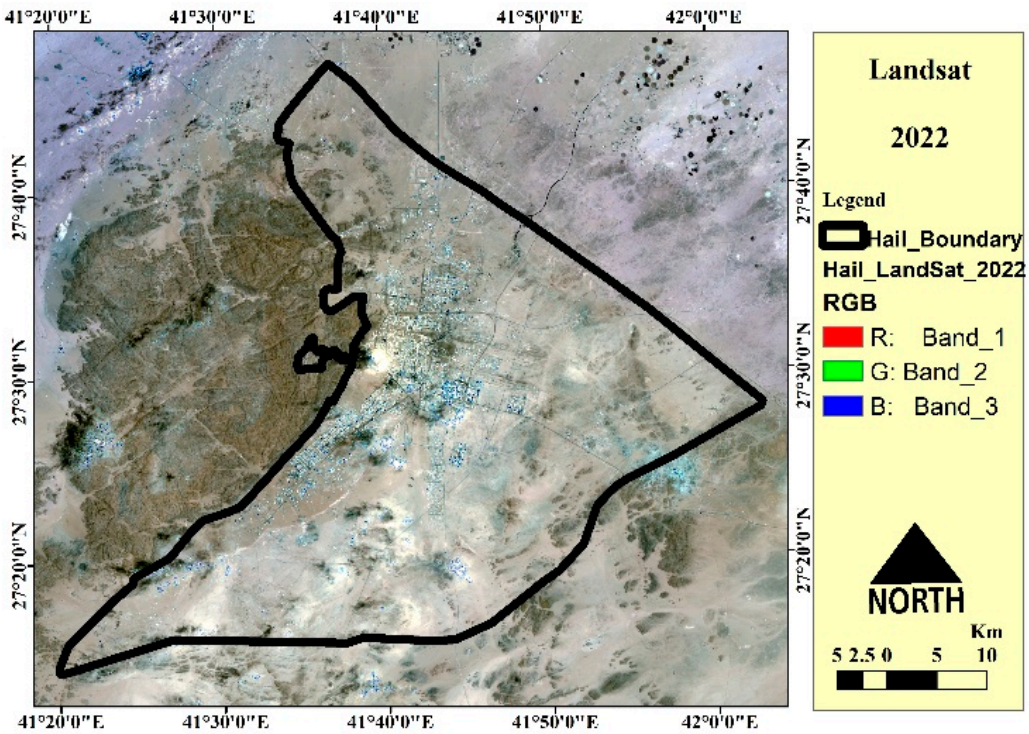

Figure 7. Satellite image (Landsat 2022) for the study area.

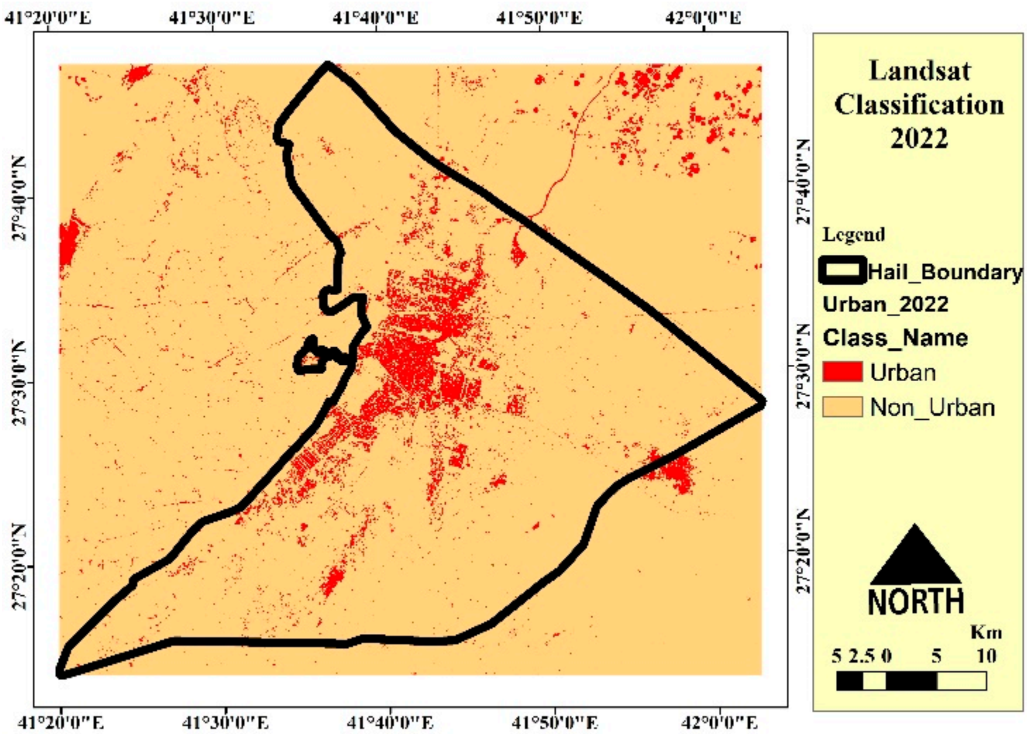

Figure 8. Landsat classification for an urban area, 2022.

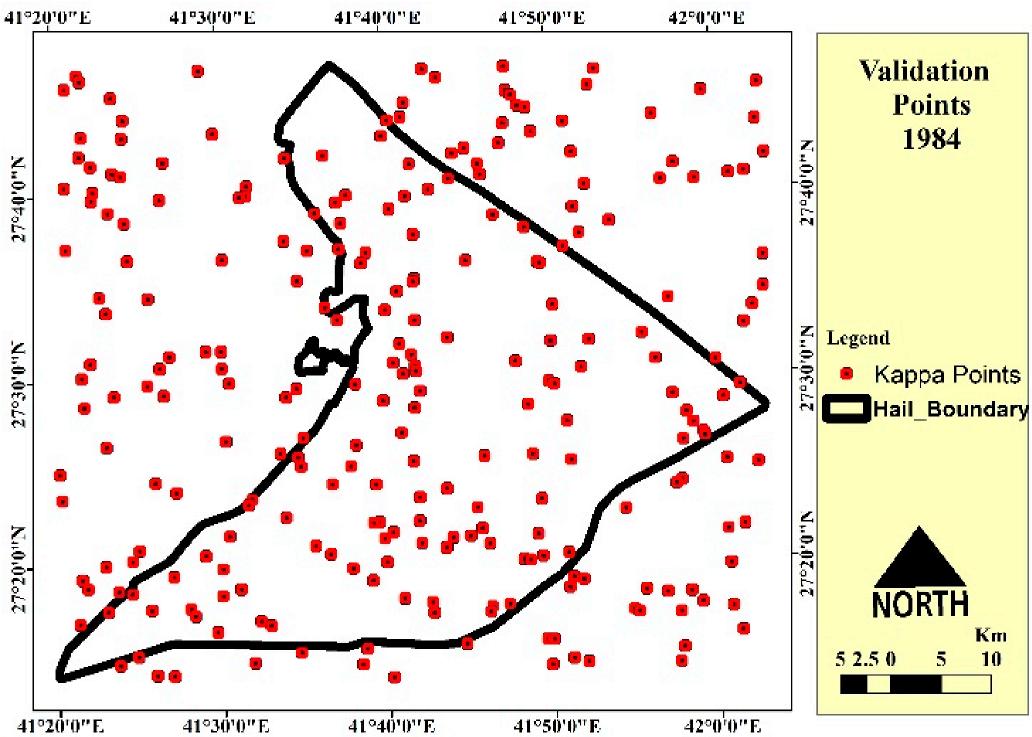

Figure 9. Distribution of Kappa validation points for 1984.

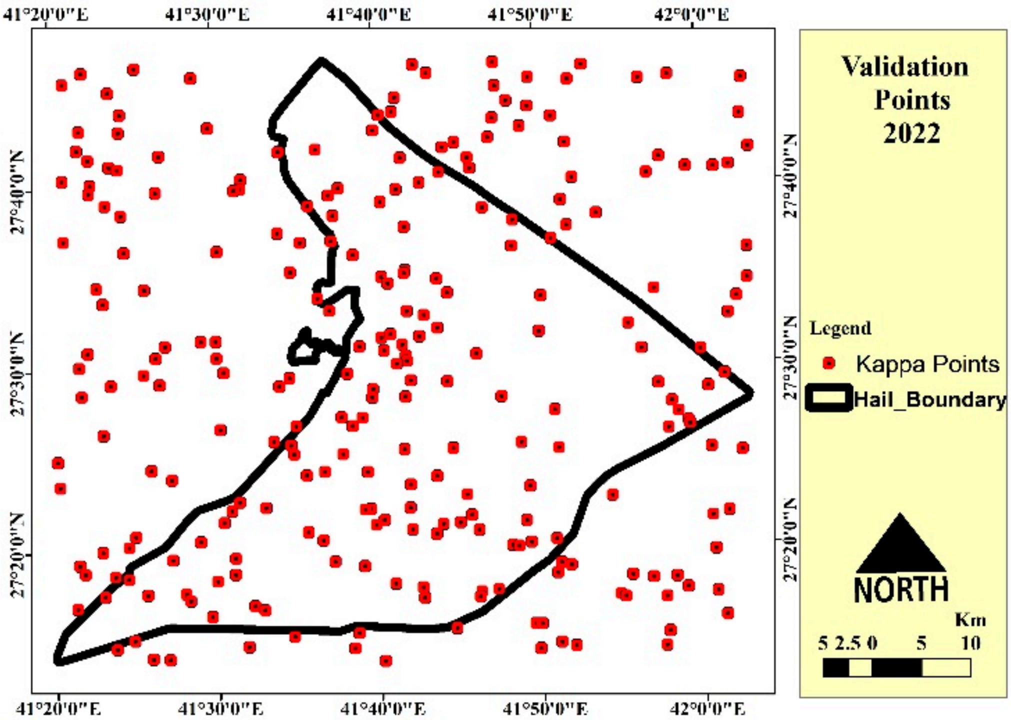

Figure 10. Distribution of Kappa validation points for 2022.

Table 3. Kappa results for land use classification, 1984.

Class Value	Urban	Non-Urban	Total	U Accuracy	Kappa
Urban	29.00	5.00	34.00	0.85	0.00
Non-Urban	2.00	221.00	223.00	0.99	0.00
Total	31.00	226.00	257.00	0.00	0.00
P Accuracy	0.94	0.98	0.00	0.97	0.00
Kappa	0.00	0.00	0.00	0.00	0.88

Table 4. Kappa results for land use classification, 2022.

Class Value	Urban	Non-Urban	Total	U Accuracy	Kappa
Urban	50.00	3.00	53.00	0.94	0.00
Non-Urban	4.00	200.00	204.00	0.98	0.00
Total	54.00	203.00	257.00	0.00	0.00
P Accuracy	0.93	0.99	0.00	0.97	0.00
Kappa	0.00	0.00	0.00	0.00	0.92

The uses of the land in Hail city may be classified as either urban or non-urban, and they were segregated into these two categories. In 1984, non-urban land use made up 97.99 percent of the total area in Hail City. This made it the most frequent type of land use in the city. According to Figures 11 and 12 That were provided, the information that is displayed in Table 5 Indicates that in the year 2022, the non-urban areas accounted for 90.60 percent of the region's total land area, while the urban regions accounted for 9.40 percent of the region's total land area. During the course of 38 years, the urban area expanded from 3454 hectares to 16,123 ha. This study focused on urban areas for the purpose of estimating the exposure area that is susceptible to the hazard of flash flooding; the total area of the urban class in this study was 171,603 ha.

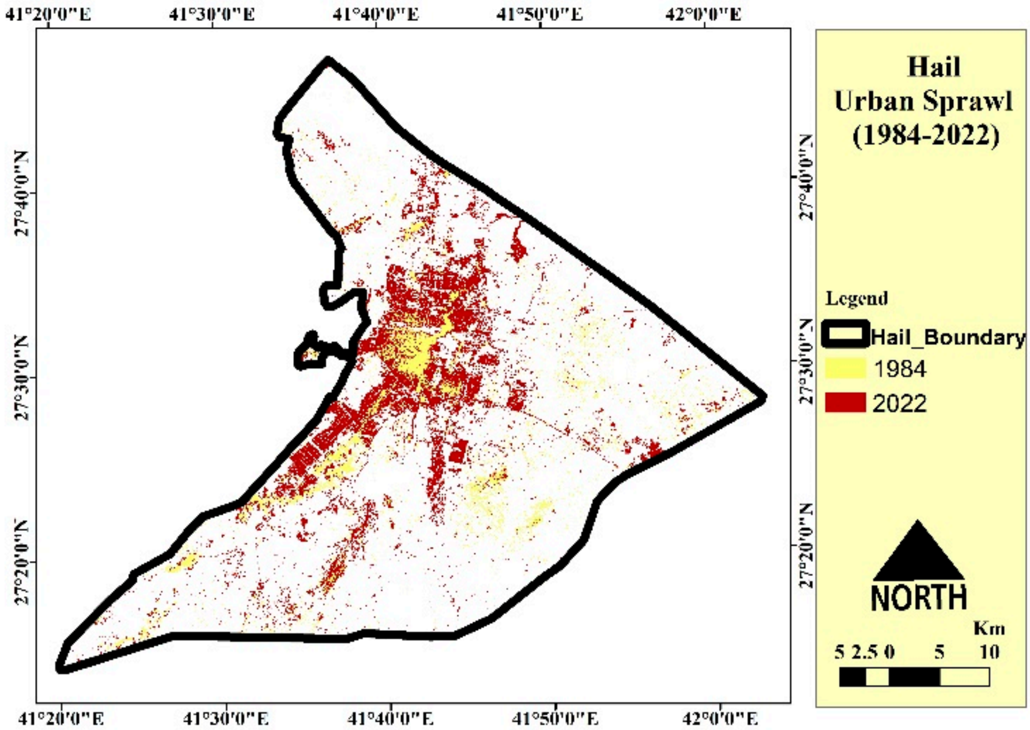

Figure 11. The urban sprawl for Hail between 1984 and 2022.

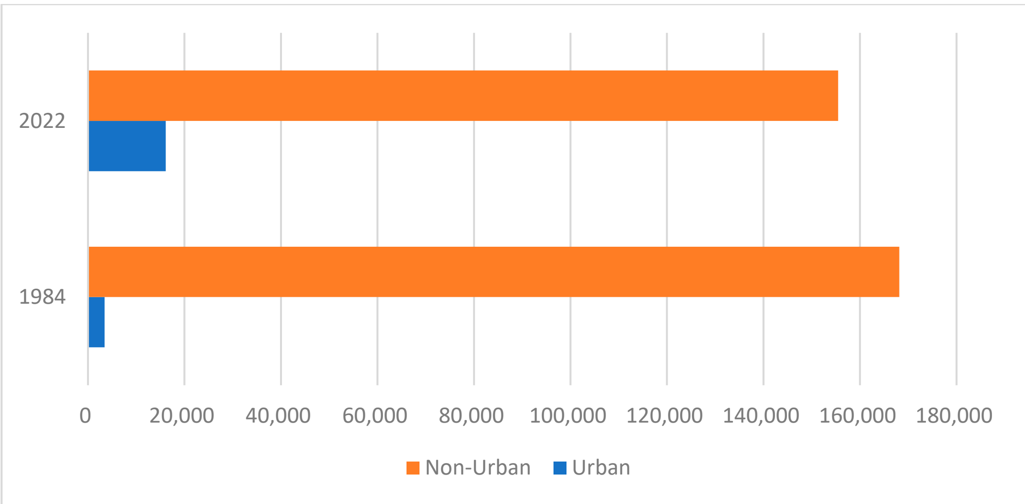

Figure 12. Urban area for Hail between 1984 and 2022.

Table 5. Landsat classification results values.

Year	Urban (Ha)	%	Non-Urban (Ha)	%	Total
1984	3454	2.01	168,149	97.99	171,603
2022	16,123	9.40	155,480	90.60	171,603

5.2. Simulating the Flash Flooding

The information obtained from the simulation exercise, such as the peak flow rates, the volume of rainfall, and the amount that was left on the surface, provided valuable insights into the possibility of predicting water flow. The information that was gathered on the connection between time and the flow of water was helpful in pinpointing the most critical point of the simulated disaster. The findings of the simulation, in which the depth of the water was estimated every 15 min, allowed for the determination of the depth of the water during peak runoff for each watershed. For the purposes of the study, the water depth file (a raster) was exported from WMS and imported into ArcGIS as seen in Figure 13.

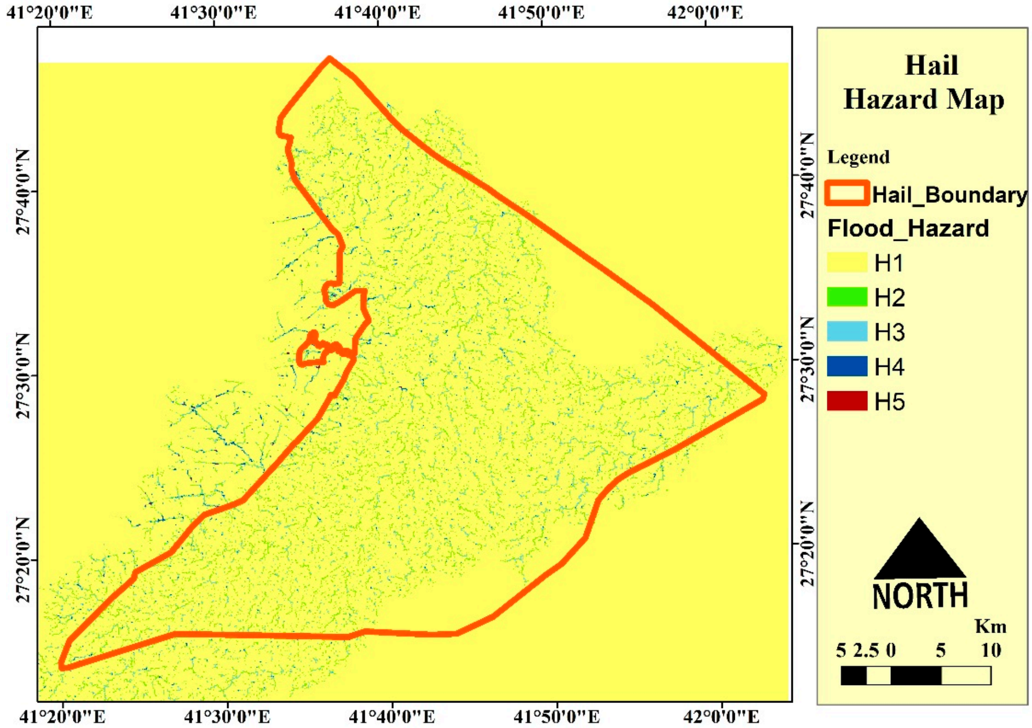

Figure 13. Hazard map of Hail city.

After converting the raster file of water depth to a vector file as the first step in ArcGIS, the next step was to divide the water depth into five different categories of hazard. These categories were Very Low Hazard (H1), Low Hazard (H2), Moderate Hazard (H3), and High Hazard (H4). Very High Hazard (H5) was the final category. The last phase was the assignment of new attributes in the urban area data file for each building to illustrate the level of hazard, based on its location from the hazard level area, as shown in Figure 13 This was the following step in the process.

5.3. Comparing the Worst-Case Historical Event between 1984-2022

Urban areas in the study area were distributed according to five categories and at the same time, the urban areas in the case study were divided into two groups based on the year (1984 and 2022) as shown in Table 6. In the risk area, urban areas allocated in the H1 zone were the biggest category in both years, occupying 3156.15 ha or about 91.39% of the risk area in the year 1984. However, it was increasing to 14,394.68 ha in 2022 with a decrease in the percentage of total urban areas of 89.28%, while the urban area for the other four classes H2, H3, H4, and H5 increased in both the net area and percentage from the total urban areas. Table 7, Figures 14 and 15 show that the biggest two categories in hazard degrees gained big urban areas located in risk zones, and it can be observed that the Extreme (H5) degree increased from 0.13 ha to 1.52 ha while the High (H4) degree has huge urban areas increasing more than 6.6 times from 11.23 ha to 74.33 ha.

In this part of the research, the results have been presented to illustrate the comparison between the exposure of urban areas in 1984 to the risks of floods and simulating the same conditions if they were repeated in 2022 after a large urban growth. The most important part of the comparison was the study of changes in urban areas in each classification individually. Figures 14 and 15 show some crucial information, the most crucial of which is that between

1984 and 2022, the rate of urbanization increased at a rate of about 467%. However, closer examination reveals that this percentage precisely reflects the rise in urban areas that are susceptible to flash flooding risks in the first classification, which was only 456%. This is made abundantly clear in Figure 16a, whereas the rest of the classifications exhibited a significant degree of variation in the rates of increase, and this can be seen in the urban increase at risk from the second classification, where the increase rate amounted to 577% and rose from 210.34 hectares to 1213.06 hectares with an increase of about 1002.72 hectares as shown in Figure 16b. This classification was not the largest, but the increase continued in the third and fourth classifications as shown in Figure 16c,d with bigger rates of 580% and 662%, respectively; nonetheless, the observed increase that raises many worries is the large increase rate. The number of urban areas that fell into the fifth classification increased by 1.169% between 1984 and 2022, as shown in Figure 16e. This is a very high rate of growth, which means that the number of urban areas exposed to the highest level of flood risk is going up by 30% every year.

Table 6. Urban areas exposure, 1984.

Flood Hazard	Hazard Degree	Water Depth	Urban Area 1984		Urban Area 2022	
			(Ha)	%	(Ha)	%
H1	Very Low	<0.5	3156.15	91.39%	14,394.68	89.28%
H2	Low	0.5–1	210.34	6.09%	1213.06	7.52%
H3	Medium	1–2	75.68	2.19%	439.28	2.72%
H4	High	2–5	11.23	0.33%	74.33	0.46%
H5	Extreme	>5	0.13	0.00%	1.52	0.01%
	Total		3453.53	100%	16,122.87	100%

Table 7. Analyzing of urban areas exposure between 1984 and 2022.

Flood Hazard	1984	2022	Differences	Increasing (1984 to 2022)
H1	3156.15	14,394.68	11,238.53	456%
H2	210.34	1213.06	1002.72	577%
H3	75.68	439.28	363.6	580%
H4	11.23	74.33	63.1	662%
H5	0.13	1.52	1.39	1169%
Total %	3453.53	16,122.87	12,669.34	**467%**

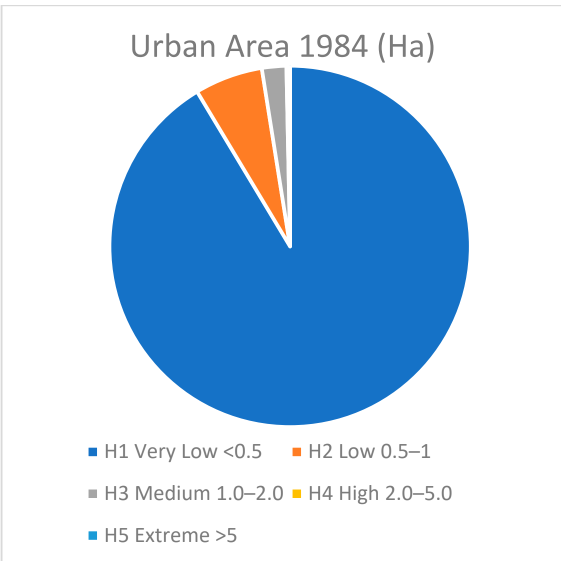

Figure 14. Distribution of urban areas exposure over hazard classes for 1984.

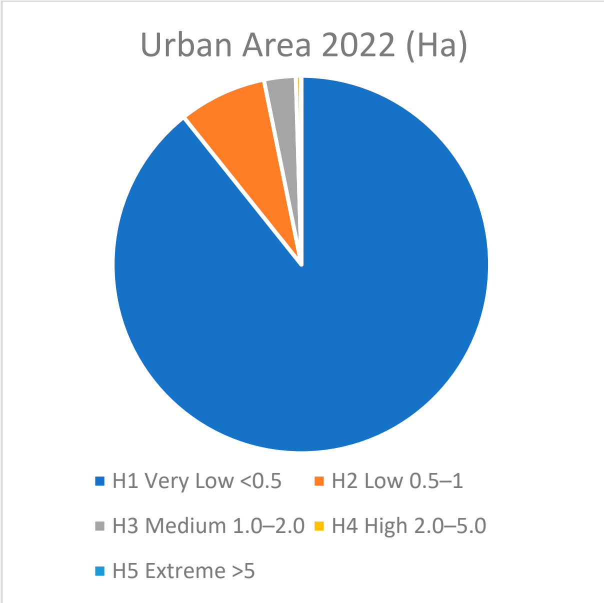

Figure 15. Distribution of urban areas exposure over hazard classes for 2022.

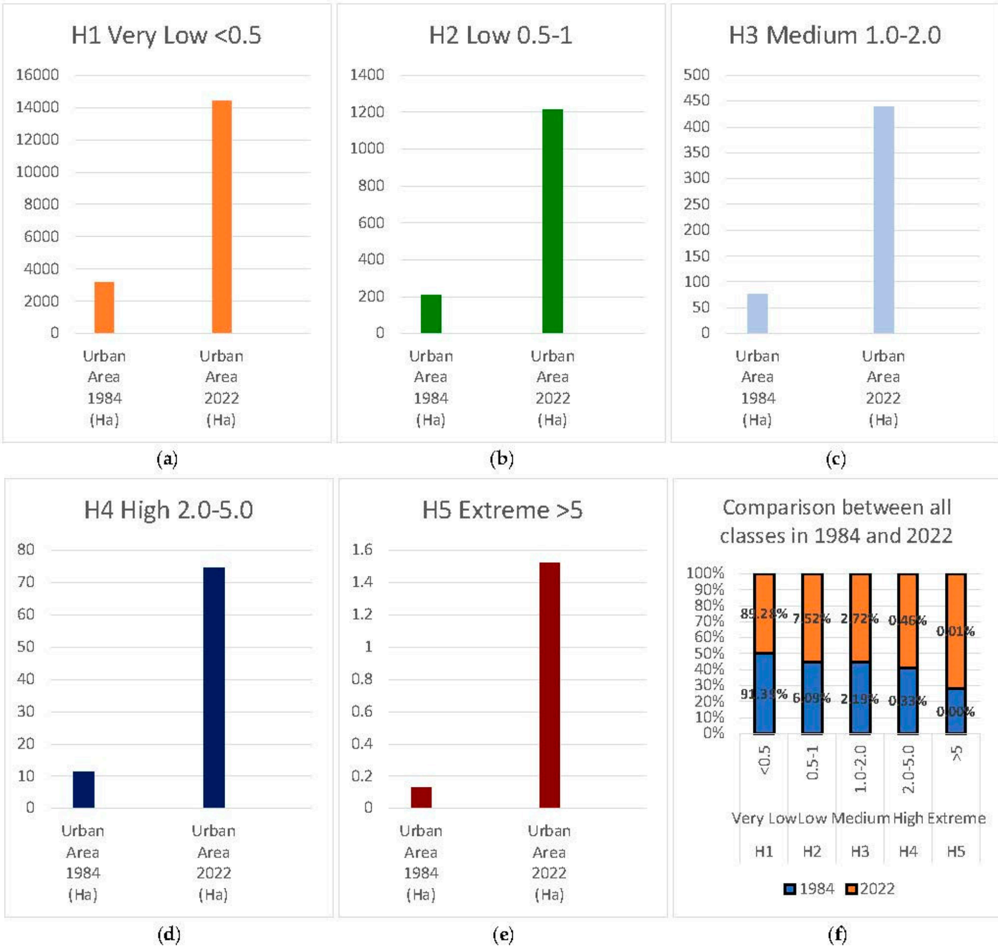

Figure 16. Urban areas exposure overall hazard classes 1984 and 2022.

6. Discussion

The authors of this paper believe that the findings of this study can be interpreted as both valuable and novel. This conclusion was reached after comparing the results of this study with those of the literature review. There are many studies use our model in a similar area in developing countries, but they use different conditions or data sources so that it is difficult to compare the same results with that [63–65]. To the best of the authors' knowledge, no other study has addressed integrated approaches to handle the problem that has been taken into consideration; this integration includes three primary distinctions: Firstly, this study was able to benefit from integrating the supervised classification in GIS with satellite images as remote sensing data in order to provide an effective way to study urban changes during separate periods of time that reached about 38 years in the study area. This is different from many previous studies [52,61,66], which were based on field study data and could not cover such a long-time span. They were also unable to examine the urban situation in 1984 and how much it has changed since then. Furthermore, the methodology of this study provided a method based on free and easy-access data for all planners and researchers, as compared to other studies that require official procedures and various permits to obtain it, and then only provide the urban areas in the current situation or some of the last few years, and it will never reach the year of study in 1984. This is because the methodology used in this study was based on free and easy-access data for all planners and researchers.

Second, the findings of this study demonstrated a significant potential for modelling the flash floods that occurred in the area under investigation by making use of the GSSHA model. The model's distinctiveness was shown by demonstrating its high level of compatibility with GIS data. In addition to GSSHA, there are numerous other numerical models that can be used to simulate flood situations. Some examples of these models include MIKE FLOOD, CCHE, FLO-2D, and TUFLOW [19]. None of the flood models described above have related to a geographic information system (GIS) in such a way that a user may rapidly adjust boundary conditions, run, and archive a flood simulation for various levee breach scenarios within a geodatabase. Furthermore, GSSHA provides many data sources available that are both free and simple to use. A digital elevation model and soil maps for all parts of the world are among the data sources. These data sources enable researchers and planners to study a wide range of phenomena remotely and without incurring a large financial burden, while still providing results of adequate accuracy [42,51,65].

Finally, the findings of this study focused on re-simulating a particular historical event that took place in 1984 and was responsible for the greatest amount of rainfall and flash floods that took place in the city of Hail. In addition to analyzing urban areas at the time of this disaster and the extent to which they were affected by torrential rains, which previous studies did not do [41,46,51,61]. The results of this paper focused on studying the extent of the impact that this natural disaster had. Within the researchers' knowledge, the research was not satisfied with that; rather, it analyzed the impact that a recurrence of such a calamity with the same conditions would have on sprawling urban areas in 2022. A comparison was then made between the exposure of urban areas to flash flood hazards, whether in the year of their occurrence in 1984 or in the incident of their recurrence in 2022, and the extent of the changes occurring in the proportions of urban distribution over the five risk zones, whereas previous studies focused on the hydrological and geographical studies of water basins [48,50].

7. Conclusions

The city of Hail is occasionally put in danger by the possibility of flash floods, which can result in the loss of lives as well as property, in addition to causing damage to structures and disruption of services. According to the findings of this study, urban expansion has persisted even in regions that are at risk of being affected by torrential downpours. This pattern was reflected in the increase in urban areas between 1984 and 2022. When modelling flash floods, the use of freely available data can produce main results that are highly realistic in nature. The method would be helpful to decision-makers and planners in countries that either do not have enough data or do not have sufficient funding to bid on development projects. This is especially true in situations where it is necessary to perform simulations of the potential site in order to reduce the risk of natural disasters. It would be extremely helpful if more precise data were available since this would make it possible to conduct more accurate simulations, which in turn would produce more trustworthy data from the analysis of the risks in the risk region. This would have a significant impact on the valuation of the land for the proposed development if it were taken into consideration.

There are many diverse types of urban expansion, but one that puts people and their belongings in harm's way is the sprawl that moves toward places that are more likely to be struck by natural disasters. According to the findings of this research study, throughout the years 2001 to 2013, urban sprawl in the area that served as the case study moved closer and closer to a risk zone that was prone to flash floods and posed varied degrees of danger.

This study focuses on two primary aspects of methodology: the first addresses the question of how to identify urban land use through the application of supervised classification to satellite imagery obtained from Landsat; however, to verify this part, it is recommended that a field survey be carried out first in order to determine which areas of the city are considered to be more historic. Following this step, a comparison between the field observations and supervised classification for satellite imagery received from Landsat can be carried out. A decent indication of the urban sprawl would be provided by this. At the same time, the differences between the two methodologies would assist researchers in calibrating the remote sensing data analyses that may be employed to acquire a result quickly and at no cost.

The second technique shows how the hazard regions were located by employing the GSSHA model found in the WMS software to simulate flash floods. For this section, we have two recommendations for how to verify the simulation: the first one is to use the same data with different hydrological software, such as CCHE, MIKE FLOOD, TUFLOW, or FLO-2D; the second suggestion is to use field study data and high-resolution data using the same apps and model, such as those of DEM, Soil Type map, and Land Use map. These data sets are not obtainable in developing countries and require a very large budget for researchers.

By modelling flash floods in risky locations, different methods for the planning of urban growth can be investigated, and this could form the basis for policy suggestions for sustainable urban development. In addition, we strongly suggest that the GSSHA model be utilized to locate the locations that are in danger of being affected by flash flooding in order to generate a preliminary estimate quickly. However, to obtain more precise results, it would be necessary to conduct analyses based on high-resolution data, which could only be obtained by incurring more costs. In the future, a study on urban sprawl in this region will make it possible to have a better understanding of the degree to which new urban areas will be at risk of being impacted by the possibility of storms and floods. It is possible that the following factors contributed to the study's limitations: (1) the resolution of data is not high resolution because all data in this study are free; (2) the frequency with which the field study I case study area was examined was too low to allow for a thorough examination of the city's various land uses; and (3) there was insufficient funding to purchase high-resolution data. We can only hope that the results of this research will assist in reducing the number of lives lost and the amount of property that was destroyed.

Author Contributions: Conceptualization, O.H. and A.R.; methodology, O.H.; M.H.H.A. and A.R.; software, O.H., validation, M.H.H.A. and O.H.; formal analysis, O.H. and A.R.; investigation, O.H. and A.R.; resources, M.A. (Mohammed Alshenaifi) and E.N.; data curation, M.A. (Mohammed Alshenaifi), K.E. and E.N.; writing—original draft preparation, O.H.; writing—review and editing, M.H.H.A. and M.T.; visualization, M.A. (Mohammed Alghaseb) and K.E.; supervision, M.H.H.A. and A.R.; project administration, M.H.H.A.; funding acquisition, M.H.H.A. All authors have read and agreed to the published version of the manuscript.

Funding: This research was funded by the Research Deanship at the University of Hail—Saudi Arabia through project number RG-21 066.

Data Availability Statement: Not applicable.

Conflicts of Interest: The authors declare no conflict of interest.

References

1. Vaz, E.; Nijkamp, P. Gravitational forces in the spatial impacts of urban sprawl: An investigation of the region of Veneto, Italy. *Habitat Int.* **2015**, *45*, 99–105. [CrossRef]
2. Jiao, L. Urban land density function: A new method to characterize urban expansion. *Landsc. Urban Plan.* **2015**, *139*, 26–39. [CrossRef]
3. Belal, A.A.; Moghanm, F.S. Detecting urban growth using remote sensing and GIS techniques in Al Gharbiya governorate, Egypt. *Egypt. J. Remote Sens. Space Sci.* **2011**, *14*, 73–79. [CrossRef]
4. Hamdy, O.; Zhao, S.; Abd El-Atty, H.; Ragab, A.; Salem, M. Urban areas management in developing countries: Analysis of the urban areas crossed with risk of storm water drains, Aswan-Egypt. *Int. J. Urban Civ. Eng.* **2020**, *14*, 96–102.
5. Yue, W.; Liu, Y.; Fan, P. Measuring urban sprawl and its drivers in large Chinese cities: The case of Hangzhou. *Land Use Policy* **2013**, *31*, 358–370. [CrossRef]
6. Lagarias, A. Urban sprawl simulation linking macro-scale processes to micro-dynamics through cellular automata, an application in Thessaloniki, Greece. *Appl. Geogr.* **2012**, *34*, 146–160. [CrossRef]
7. Guha-Sapir, D.; Vos, F.; Below, R. *Annual Disaster Statistical Review 2011*; Centre for Research on the Epidemiology of Disasters: Brussels, Belgium, 2012; p. 52.
8. IPCC. *IPCC Sixth Assessment Report*; IPCC: Geneva, Switzerland, 2022.
9. Güneralp, B.; Güneralp, İ.; Liu, Y. Changing global patterns of urban exposure to flood and drought hazards. *Glob. Environ. Chang.* **2015**, *31*, 217–225. [CrossRef]
10. World Bank Group. Egypt Dashboard. Available online: http://sdwebx.worldbank.org/climateportalb/home.cfm?page=country_profile&CCode=EGY&ThisTab=NaturalHazards (accessed on 11 September 2022).
11. United Nations Office for Disaster Risk Reduction. *National Strategy for Crisis/Disaster Management and Disaster Risk Reduction*; United Nations Office for Disaster Risk Reduction: Geneva, Switzerland, 2010.
12. Hamdy, O.; Zhao, S.; Salheen, M.; Eid, Y. Using Arc GIS to analyse urban growth towards torrent risk areas (Aswan city as a case study). *IOP Conf. Ser. Earth Environ. Sci.* **2014**, *20*, 12009. [CrossRef]
13. Ayyub, B.M. *Risk Analysis*; The United Nations Office for Disaster Risk Reduction: Geneva, Switzerland, 2014.
14. Twigg, J. *Disaster Risk Reduction*; Humanitarian Policy Group: London, UK, 2015.
15. APFM. Guidance on Flash Flood Management. Recent experiences from Central and Eastern Europe. In *Flood Management Tools Series*; APFM: Seattle, DC, USA, 2007. Available online: https://www.preventionweb.net/publication/guidance-flash-flood-management-recent-experiences-central-and-eastern-europe (accessed on 11 September 2022).
16. Tanner, D. Analyzing wildlife habitat with Google Earth. *Green Teach.* **2009**, *87*, 9–15.
17. Wilson, C.R.; Murphy, J.; Trautmann, N.M.; Makinster, J.G. From Local to Global: A Birds-Eye View of Changing Landscapes. *Am. Biol. Teach.* **2009**, *71*, 412–416. [CrossRef]
18. McCarty, J.A., Jr. *Long-term Simulation in Parley's Canyon Using GSSHA*; Brigham Young University: Provo, UT, USA, 2013.
19. Paudel, M. *An Examination of Distributed Hydrologic Modeling Methods as Compared with Traditional Lumped Parameter Approaches*; Brigham Young University: Provo, UT, USA, 2010.
20. Taylor, J.R.; Lovell, S.T. Mapping public and private spaces of urban agriculture in Chicago through the analysis of high-resolution aerial images in Google Earth. *Landsc. Urban Plan.* **2012**, *108*, 57–70. [CrossRef]
21. Collin, A.; Nadaoka, K.; Nakamura, T. Mapping VHR Water Depth, Seabed and Land Cover Using Google Earth Data. *ISPRS Int. J. Geoinf.* **2014**, *3*, 1157–1179. [CrossRef]
22. El Hassan, A.A.; Sharif, H.O.; Jackson, T.; Chintalapudi, S. Performance of a conceptual and physically based model in simulating the response of a semi-urbanized watershed in San Antonio, Texas. *Hydrol. Process.* **2012**, *27*, 3394–3408. [CrossRef]
23. Wright, D.B.; Smith, J.A.; Baeck, M.L. Flood frequency analysis using radar rainfall fields and stochastic storm transposition. *Water Resour. Res.* **2014**, *50*, 1592–1615. [CrossRef]
24. Noby, M.; Michitaka, U.; Hamdy, O. Urban Risk Assessments: Framework for Identifying Land-uses Exposure of Coastal Cities to Sea Level Rise, a Case Study of Alexandria. *SVU-Int. J. Eng. Sci. Appl.* **2022**, *3*, 78–90. [CrossRef]
25. Rikimaru, P.A.; Roy, P.S.; Miyatake, S. Tropical Forest cover density mapping. *Trop. Ecol.* **2002**, *43*, 39–47.
26. Ramadhan Kete, S.C.; Suprihatin Tarigan, S.D.; Effendi, H. Land use classification based on object and pixel using Landsat 8 OLI in Kendari City, Southeast Sulawesi Province, Indonesia. *IOP Conf. Ser. Earth Environ. Sci.* **2019**, *284*, 012019. [CrossRef]
27. Schneider, A. Monitoring land cover change in urban and peri-urban areas using dense time stacks of Landsat satellite data and a data mining approach. *Remote Sens. Environ.* **2012**, *124*, 689–704. [CrossRef]
28. USGS, "GloVis—USGS". 2001. Available online: https://glovis.usgs.gov/ (accessed on 2 October 2022).
29. Hamdy, O.; Zhao, S.; Salheen, M.A.; Eid, Y.Y. Identifying the Risk Areas and Urban Growth by ArcGIS-Tools. *Geosciences* **2016**, *6*, 47. [CrossRef]

30. Stefanidis, S.; Alexandridis, V.; Mallinis, G. A cloud-based mapping approach for assessing spatiotemporal changes in erosion dynamics due to biotic and abiotic disturbances in a Mediterranean Peri-Urban forest. *Catena* **2022**, *218*, 106564. [CrossRef]
31. Cohen, B. Urban growth in developing countries: A review of current trends and a caution regarding existing forecasts. *World Dev.* **2004**, *32*, 23–51. [CrossRef]
32. Hamdy, O.; Gaber, H.; Abdalzaher, M.S.; Elhadidy, M. Identifying exposure of urban area to certain seismic hazard using machine learning and GIS: A case study of greater Cairo. *Sustainability* **2022**, *14*, 10722. [CrossRef]
33. Alsonny, Z.; Ahmed, A.M.M.A.; Hamdy, O. Studying the Effect of Urban Green Spaces Location on Urban Heat Island in Cities Using Remote Sensing Techniques, 6th October City as a Case Study. *Int. Des. J.* **2022**, *12*, 243–262.
34. Van Vliet, J.; Bregt, A.K.; Hagen-Zanker, A. Revisiting Kappa to account for change in the accuracy assessment of land-use change models. *Ecol. Modell.* **2011**, *222*, 1367–1375. [CrossRef]
35. Hamdy, O. Using Remote Sensing Techniques to Assess the Changes in the Rate of Urban Green Spaces in Egypt: A Case Study of Greater Cairo. *Int. Des. J.* **2022**, *12*, 53–64. [CrossRef]
36. Alsonny, Z.; Hamdy, O. Procedural Framework for Assessing the Impact of New Cities Growth on Urban Heat Island, A Case Study of 6thOctober City. *SVU-Int. J. Eng. Sci. Appl.* **2022**, *3*, 64–78. [CrossRef]
37. Hamdy, O.; Alsonny, Z. Assessing the Impacts of Land Use Diversity on Urban Heat Island in New Cities in Egypt, Tiba City as a Case Study. *Int. Des. J.* **2022**, *12*, 93–103. [CrossRef]
38. A Draft Guide to Flood Risk Assessment Data Collection Survey on ASEAN regional Collaboration in Disaster Management. Available online: https://openjicareport.jica.go.jp/216/216/216_100_12085734.html (accessed on 11 September 2022).
39. Accuracy Assessment for Image Classification—ArcMap. Documentation. Available online: https://desktop.arcgis.com/en/arcmap/latest/manage-data/raster-and-images/accuracy-assessment-for-image-classification.htm (accessed on 27 December 2021).
40. ESRI. Compute Confusion Matrix (Spatial Analyst)—ArcMap. Documentation. Available online: https://desktop.arcgis.com/en/arcmap/latest/tools/spatial-analyst-toolbox/compute-confusion-matrix.htm (accessed on 27 December 2021).
41. Hereher, M.E. Synopsis of geo-environmental hazards in Hail region, Saudi Arabia using remote sensing. *Environ. Earth Sci.* **2016**, *75*, 1–13. [CrossRef]
42. Al Saud, M. Assessment of flood hazard of Jeddah area 2009, Saudi Arabia. *J. Water Resour. Prot.* **2010**, *2*, 839–847. [CrossRef]
43. Youssef, A.M.; Pradhan, B.; Sabtan, A.A.; El-Harbi, H.M. Coupling of remote sensing data aided with field investigations for geological hazards assessment in Jazan area, Kingdom of Saudi Arabia. *Environ. Earth Sci.* **2012**, *65*, 119–130. [CrossRef]
44. Youssef, A.M.; Maerz, N.H. Overview of some geological hazards in the Saudi Arabia. *Environ. Earth Sci.* **2013**, *70*, 3115–3130. [CrossRef]
45. Alharbi, T.; Sultan, M.; Sefry, S.; Elkadiri, R.; Ahmed, M.; Chase, R.; Milewski, A.; Abu Abdullah, M.; Emil, M.; Chounaird, K. An assessment of landslide susceptibility in the Faifa area, Saudi Arabia, using remote sensing and GIS techniques. *Nat. Hazards Earth Syst. Sci.* **2014**, *14*, 1553–1564. [CrossRef]
46. Hereher, M.; Alghmdi, A.; Mseddi, K.; el Kenawy, A. Remote sensing of vegetation prolonged drought at the salt playas of Hail—Saudi Arabia. *Egypt. J. Remote Sens. Space Sci.* **2022**, *25*, 135–145. [CrossRef]
47. Ahmed, I.; Nazzal, Y.; Zaidi, F. Groundwater pollution risk mapping using modified DRASTIC model in parts of Hail region of Saudi Arabia. *Environ. Eng. Res.* **2018**, *23*, 84–91. [CrossRef]
48. Al-Sehly, T.E.; Youssef, A.M.; Al-Otaibi, A.A.; Al-Harbi, H.M. Site investigation using engineering geology mapping and geological hazard evaluation: Case study of the New Hail Economic City, Hail Region, KSA. In Proceedings of the International Congress and Exhibition, Sustainable Civil Infrastructures: Innovative Infrastructure Geotechnology, El-Salam, Egypt, 15 July 2017; pp. 1–19.
49. Alhedyan, M.A. Change Detection of Land Use and Land Cover, Using Landsat-8 and Sentinel-2A. Ph.D. Dissertation, University of Leicester, Leicester, UK, 2021.
50. Sharaf, M.A.; Hussein, M.T. Groundwater quality in the Saq aquifer, Saudi Arabia. *Hydrol. Sci.* **1996**, *4*, 683–699. [CrossRef]
51. Elshewey, M.I.A. The Study of Prevention of the Dangers of the Torrents and Draining Rainwater of Uqdah in Hail Region, Saudi Arabia. *Int. J. Appl. Innov. Eng. Manag.* **2016**, *5*, 62–75.
52. Pienaar, H.; Fundarò Costanza, S.; Mantia, L.; Nguyen, H.A. *Future Saudi Cities Programme City Profiles Series: Hael*; 2019. Available online: https://saudiarabia.un.org/en/39461-future-saudi-cities-programme-city-profiles-series-abha (accessed on 27 December 2021).
53. El Kenawy, A.M.; Mccabe, M.F. A multi-decadal assessment of the performance of gauge- and model-based rainfall products over Saudi Arabia: Climatology, anomalies and trends. *Int. J. Climatol.* **2016**, *36*, 656–674. [CrossRef]
54. Do, H.-T.; Limet, S.; Melin, E. Parallel Computing Flow Accumulation in Large Digital Elevation Models. *Procedia Comput. Sci.* **2011**, *4*, 2277–2286. [CrossRef]
55. Jarihani, A.A.; Callow, J.N.; McVicar, T.R.; van Niel, T.G.; Larsen, J.R. Satellite-derived Digital Elevation Model (DEM) selection, preparation and correction for hydrodynamic modelling in large, low-gradient and data-sparse catchments. *J. Hydrol.* **2015**, *524*, 489–506. [CrossRef]
56. Small, C.; Sohn, R. Correlation scales of digital elevation models in developed coastal environments. *Remote Sens. Environ.* **2015**, *159*, 80–85. [CrossRef]

57. ESRI. Classifying Landsat Image Services to Make a Land Cover Map. Available online: https://www.esri.com/arcgis-blog/products/product/imagery/classifying-landsat-image-services-to-make-a-land-cover-map/ (accessed on 27 December 2021).
58. Tran, H.L. *A GIS-Based Data Model and Tools for Analysis and Visualization of Levee Breaching Using the GSSHA Model*; Brigham Young University: Provo, UT, USA, 2011.
59. Hall, S.R. *Model Development and Calibration for a Flood Early Warning System*; Brigham Young University: Provo, UT, USA, 2013.
60. Hamelin, J. *Estimation of GSSHA (Gridded Surface/Subsurface Hydrologic Analysis) Model Parameters for Chotysanka Basin Using a Long Term Simulation*; Czech Technical University of Prague: Prague, Czech Republic, 2013.
61. Almashat, H.; AlSharqawy, M. The Dangers of Torrential Rains in the Al-Adeira Valley Basin in the Hail Region: An Applied Study Using GIS and Remote Sensing Techniques. 2017, pp. 1–19. Available online: http://swideg-geography.blogspot.com/2018/03/blog-post_69.html#.Y2bsn3ZBzWV. (accessed on 6 November 2022).
62. Audigé, L.; Bhandari, M.; Kellam, J. How reliable are reliability studies of fracture classifications? A systematic review of their methodologies. *Acta Orthop. Scand.* **2004**, *75*, 184–194. [CrossRef] [PubMed]
63. El-Sayed, E.A.; Habib, E. Advanced technique for rainfall-runoff simulation in arid catchments Sinai, Egypt. In Proceedings of the 3rd International Conference on Water Resources and Arid Environments, Riyadh, Saudi Arabia, 16–19 November 2008.
64. Fathy, I.; Abd-Elhamid, H.F.; Negm, A.M. Prediction and mitigation of flash floods in Egypt. In *Flash Floods in Egypt*; Springer: Berlin/Heidelberg, Germany, 2020; pp. 349–368.
65. Hamdy, O.; Zhao, S. A Study on Urban Growth in Torrent Risk Areas in Aswan, Egypt. *J. Archit. Plan. Trans. AIJ* **2016**, *81*, 1733–1741. [CrossRef]
66. Al-Hawas, F. The Archaeological and Architectural Remains of the Ancient City of Faid in the Province of Hail in Saudi Arabia. Ph.D. Dissertation, University of Southampton, Southampton, UK, 2003.